Jurnal Polimesin
Department of Mechanical Engineering
State Polytechnic of Lhokseumawe
http://e-jurnal.pnl.ac.id/polimesin

e-ISSN	: 2549-1999	No.	: 3	Month	: June
p-ISSN	: 1693-5462	Volume	: 23	Year	: 2025

Processing dates: received on 2025-04-29, reviewed on 2025-06-26, accepted on 2025-06-27 and online availability on 2025-06-30

Performance analysis of buck-boost DC-DC converter with incremental conductance MPPT for PV system

Rimbawati[1,*], Wira Agus Lexmana Tanjung[1], Partaonan Harahap[1], Munawar Alfansury Siregar[2], Dultudes Mangopo[3]
[1]Departement of Electrical Engineering, Muhammadiyah University of North Sumatra, Medan-North Sumatra 20238, Indonesia
[2]Department of Mechanical Engineering, Muhammadiyah University of North Sumatra, Medan-North Sumatra 20238, Indonesia
[3]Departement of Electrical Engineering, Universitas Cenderawasih, Jayapura 99358, Indonesia
*Corresponding Author: rimbawati@umsu.ac.id

Abstract
Electric energy is essential in modern life, with solar power emerging as a leading renewable energy source. Photovoltaic (PV) systems convert sunlight into electricity, but their output is highly sensitive to environmental changes such as solar irradiance. A reliable Maximum Power Point Tracking (MPPT) method is needed to maximize efficiency. This study investigates the performance of a Buck-Boost DC-DC converter integrated with the Incremental Conductance (InCo) algorithm for MPPT in PV systems. A comparative analysis is conducted between systems with and without MPPT under variable irradiance conditions, replicating real-world scenarios like partially cloudy weather. Simulations were performed in MATLAB® and Simulink® using a PV module model based on actual datasheet parameters. A digital lux meter was used to simulate light intensity fluctuations. Results show that the MPPT-enabled system effectively tracks the Maximum Power Point (MPP) even during rapid irradiance changes. On average, the system achieved improvements of 65.53% in output voltage, 65.48% in current, and 86.47% in power compared to the non-MPPT configuration. These findings demonstrate that combining the InCo algorithm with a Buck-Boost converter offers an efficient and adaptive solution for improving energy conversion in PV systems in environments with unstable solar exposure.

Keywords:
Photovoltaic, buck-boost converter, maximum power point tracking, incremental conductance, solar irradiance

1 Introduction

Human life today heavily relies on electrical energy. Along with technological advancements, humans must continually innovate to adapt to the changes brought about by progress, particularly in meeting energy demands, especially electrical energy. As conventional energy sources such as coal and oil become increasingly scarce, the energy demand continues to rise in parallel with global population growth. However, the use of these limited conventional energy sources often leads to various energy crises, as the increasing demand for electricity is not matched by a sufficient energy supply [1],[2].

Based on projections, Indonesia's electricity demand by 2024 is expected to reach 50,000 MW. Nevertheless, this target has yet to be fully achieved. In response, the Indonesian government initiated a 35,000 MW mega project under PLN's roadmap to address the electricity gap. In 2015, the electrification ratio was approximately 84%, and with the continuous growth of the population, the need for intensified development, particularly through environmentally friendly renewable energy sources, has become even more urgent. One of the most widely adopted methods for renewable energy generation is the conversion of solar energy. A comparative study on global energy consumption released by the International Energy Agency (IEA) projects that by 2050, more than 45% of the world's energy needs will be supplied by solar power plants [3].

The use of Photovoltaic (PV) technology offers a sustainable and environmentally friendly energy source. However, successful implementation requires accurate resource potential assessments, including measurements of solar intensity[4].The efficiency of solar cell energy conversion is a fundamental factor in optimizing the performance of solar panels. The amount of power generated by a solar energy system is directly influenced by this efficiency, which itself depends on several factors: solar panel efficiency (8%–15%), inverter efficiency (95%–98%), and Maximum Power Point Tracking (MPPT) efficiency (around 98%) [5].

In recent years, various methods have been developed to improve MPPT tracking. Two of the most commonly used methods are the Perturb and Observe (P&O) method and the Incremental Conductance (InCo) method. The P&O method is simpler to implement but tends to be less accurate in tracking the Maximum Power Point (MPP) under fluctuating atmospheric conditions. In contrast, the InCo method, although more complex, can quickly adapt to changes in environmental conditions and deliver better tracking performance.

PV systems generally have relatively low efficiency because the power they generate is heavily influenced by environmental factors such as variations in irradiance and temperature. To address this issue, the MPPT system is employed to extract the maximum available power from the solar PV module. A DC-DC converter acts as the interface between the PV module and the load by adjusting the duty cycle to match the load impedance with the source impedance, thereby maximizing the extracted power. The MPP corresponds to the voltage at which the PV module delivers its highest power output. In the InCo method, the array terminal voltage is dynamically adjusted to track the MPP voltage[6][7].

Based on the explanation above, this final project proposes the implementation of an MPPT system using the InCo algorithm to optimize the output power of solar panels without requiring mechanical tracking adjustments. Additionally, a comparative analysis using Buck and Boost converters will be conducted through simulations in MATLAB® and Simulink®. In the InCo method, the MPPT control system based on the InCo algorithm connected to a buck-boost converter can optimize the PV output power, where the InCo algorithm is known to support battery safety and longevity.

The maximum operating point of PV (PV) cells varies at different voltage values depending on environmental conditions. Research indicates that the InCo method operates based on the gradient of the power-voltage (P-V) or power-current (P-I) characteristic curves of a solar cell. The InCo algorithm was developed to address limitations found in the P&O method, using the slope of the P-V curve as its control basis. Technological developments in PV energy conversion have also become increasingly diverse [8]. Advances in components and circuit technology have enabled the creation of DC power supply systems capable of converting input DC voltage into either a higher or lower output voltage.

A comprehensive review of relevant studies on research and highlighting the novelty of the current study, namely:

1. "Un Nuevo Método de Control Predictivo Basado en Modelo para Sistemas Fotovoltaicos Basados en Inversores Buck-Boost" (2022).

Presenting a control scheme based on Model Predictive Control (MPC) on a buck-boost converter for a PV system, integrated with the InCo algorithm for MPPT. Simulations show high-quality sinusoidal output (THD < 2%) and automatic battery charging/discharging capability according to irradiance 700–1000 W/m²[9].

2. Un control sin sensor de corriente del convertidor Buck-Boost para MPPT" (2022)

Proposing a sensor-less method that utilizes the mathematical objective function of the buck-boost converter and Arduino DUE. Simulation and experimental results show a reduction in computational load of about 24% and a cost efficiency of 27.95% compared to traditional P&O[10].

3. "Convertidor Buck-Boost basado en Aprendizaje Profundo para Módulos FV" (2024)

Displaying the integration of an Artificial Neural Network (ANN) to improve dynamic response and reduce overshoot compared to PID. Input data from PV (10–48 V), suitable for up to 10 kVA single-bank battery systems, shows significant performance over conventional systems [11].

4. "Convertidor Buck-Boost Multientrada Programable para–Arrays Fotovoltaicos" (2024)

A dual-switch-based multi-input topology for buck-boost converters is introduced, supporting both parallel and series PV panels flexibly and enabling MPPT for each panel. Validation through Simulink indicates a wide operating range and low switching stress[12].

5. "Análisis e Implementación del Convertidor Buck-Boost Modificado de Serie Adelante" (2024)

Focus on the isolated BBMSF (Buck-Boost Modified Series Forward) topology for DMPPT (per-panel converter) in grid-tied systems. The 225 W prototype unit shows an efficiency of up to 93.6% and the advantages of soft-switching (ZVS/ZCS) [13].

Previous studies describe buck-boost converters as electronic circuits that regulate voltage and current based on load requirements. Variations in load can shift the operating point of the solar cell (its current-voltage characteristics), which in turn affects the system's maximum output power. The buck-boost converter method focuses on stabilizing the output voltage by using Proportional-Integral (PI) control. Research has shown that buck-boost converters with PI control can achieve an efficiency of up to 9.5%, slightly outperforming PID-controlled converters in terms of efficiency, although PID provides better transient response [14].

In addition, the XL6009 buck-boost converter tested with a 12V 7Ah battery showed effective voltage regulation, achieving an average efficiency of 73.9% at 17,500 lux irradiance. Moreover, buck-boost converters are more reliable than SEPIC converters due to their simpler and more cost-effective design, as well as their faster charging capability, reportedly five minutes faster than SEPIC-based systems [15][16].

2 Materials and methods

2.1 Materials and equipment

The research "Exploration of Buck-Boost DC-DC Converter with InCo Algorithm for MPPT in PV Systems" was conducted using MATLAB® and Simulink® software simulation to determine the output of solar panels, where the data was taken from field data conducted in the Pematang Johar rice field tourism area, Jalan Johar Raya, Gg. Tanah Wakaf Jl. Dusun VI, Pematang Johar, Labuhan Deli District, Deli Serdang Regency, North Sumatra, from July to December 2020.

2.2 Solar Irradiation

Solar energy conversion is widely employed to generate electricity. The sun, with a diameter of approximately 1.39×10^9 meters, is orbited by the Earth along an elliptical path, maintaining an average distance of 1.495×10^{11} meters. Sunlight takes about 8 minutes and 20 seconds to reach Earth. The solar radiation received plays a crucial role in various applications, especially solar cells. Indonesia, located on the equator, receives abundant sunlight year-round, with an average solar radiation intensity of 4.5–4.8 kWh/m²/day across its territory[17][18].

The total solar energy reaching the Earth's surface annually amounts to 3072 joules, roughly 10,000 times greater than the world's current energy consumption. The solar constant, representing the average radiation flux density outside Earth's atmosphere, is about 1367 W/m² (within ±1%), with most radiation falling in the 0.3 to 3 μm wavelength range. Light intensity measurements are typically expressed in lux, and although there is no exact conversion between lux and W/m², an approximate value is 1 lux = 0.0079 W/m² [19][20].

Solar radiation exhibits directional characteristics determined by the angle of incidence, impacting how much energy is absorbed by a surface. Solar electromagnetic radiation spans wavelengths from 0.3 μm to over 3 μm. At noon on a clear day, solar radiation can reach 1000 W/m². A solar cell with a 10% efficiency over a 1 m² area could produce 100 W of electricity. Commercial solar modules generally have efficiency rates ranging from 5% to 15%, depending on the materials used [21][18].

2.3 PV

PV technology utilizes semiconductor materials to convert sunlight into Direct Current (DC) electricity. A typical solar cell is composed of thin semiconductor layers that absorb sunlight and generate an electric current. These cells are generally about 0.3 mm thick and consist of positive (P-type) and negative (N-type) semiconductor layers. The P-type silicon layer, coated with a nickel ring to serve as the positive terminal, is thin enough to allow sunlight to penetrate [22][23].

Beneath it, the N-type layer, also nickel-coated, acts as the negative terminal. The intensity of sunlight directly affects the current generated; thus, weather conditions play a significant role in solar cell performance. Several factors that influence PV system performance include:

1. Surface temperature of the PV module.
2. Solar radiation (irradiance).
3. Wind speed.
4. Atmospheric conditions.
5. PV module orientation.
6. The tilt angle relative to the sun.

In the silicon rod, there is a junction between the p-type and n-type regions. Therefore, it is called a p-n junction. If now, the p-type part is connected to the positive terminal of a battery, while the negative terminal is connected to the n-type part, a connection known as forward bias occurs. In that state, an electric current is generated in the circuit due to both types of charge carriers. So, the electric current flowing in the p-n junction is caused by the movement of holes, but in the opposite direction to the movement of electrons. Electrons moving within a conductor can generate electrical energy. And this electrical energy is what is called electric current, which flows in the opposite direction to the movement of the electrons. The process of Electron Liberation by a Photon can be seen in Fig. 1.

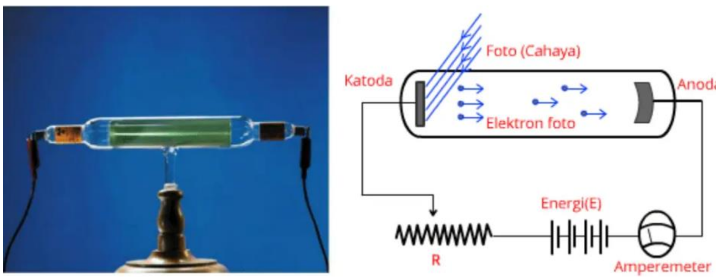

Fig. 1. The process of Electron Liberation by a Photon[18]

2.4 Equivalent circuit

Solar Panel Solar panels are used to convert solar radiation into electrical energy. Solar panels can be connected in series or parallel. The solar panel system shows non-linear I-V and P-V curves that depend on the changes in temperature and radiation present at that time. The equivalent circuit of the solar panel is represented by one current source, one diode connected in parallel with the current source, one resistor connected in parallel with the current source and the diode, one series resistor, and an output terminal. Solar panel equivalent can be seen in Fig. 2.

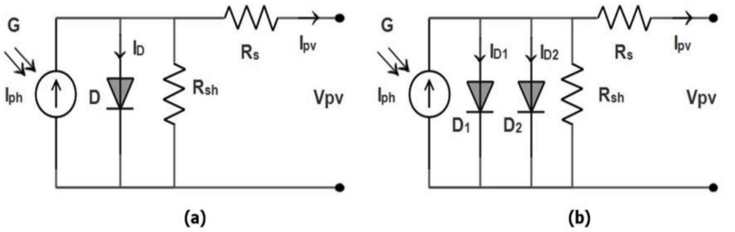

Fig. 2. Solar panel equivalent circuit (a) single diode, and (b) double diode[24]

By using analysis with Kirchhoff's Current Law on the equivalent circuit, the circuit can be represented as Eq. (1).

$$I_{Pv} = I_{Ph} - I_D - I_{Rsh} \quad (1)$$

Because the IPh current is the current generated from the process of converting light energy into electrical energy, the value of this IPh current varies depending on changes in Irradiance (λ) and the temperature of the solar cell (TC). Irradiance is the derivative of light radiation over time that represents the power generated from the electromagnetic radiation of light on a surface. The following is the Eq. (2) that represents the relationship between IPh, λ, and TC[25].

$$I_{Ph} = \left(\frac{I_{Sc}\,\lambda}{\lambda_{ref}}\right) + K_I(T_C - T_{ref}) \quad (2)$$

I_P is the current flowing in the diode and has Eq. (3).

$$I_D = I_S(\exp\left(\frac{q(V_{Pv+R_SIPV)}}{AKT_C}\right) - 1) \quad (3)$$

I_S is the saturation current of the solar cell and is related to the temperature of the solar cell according to Eq. (4) [26].

$$I_S = I_{RS}\left(\frac{Tc}{Tref}\right)^3 exp(\frac{qEG\left(\frac{1-1}{T_{ref}T_C}\right)}{KA}) \quad (4)$$

Meanwhile, the I_{RS} current, which is the reversal saturation current, can be obtained based on Eq. (5).

$$I_{Rs} = \frac{I_{SC}}{\left(\frac{qVoc}{e^{AKTc}} - 1\right)} \quad (5)$$

Then Eq. (2) can be written as Eq. (6) to obtain the characteristic equation of IPV.

$$I_{PV} = I_{Ph} - I_S\left(e\frac{q(V_{Pv+R_SIPV)}}{AKT_C} - 1\right) - \frac{V_{PV} + R_SI_{PV}}{R_{Sh}} \quad (6)$$

Explanation of the variables contained in Eqs. (1) to (6) are, I_{PV} is the solar cell output current (Ampere), I_{Ph} is the energy conversion current (Ampere), V_{PV} is the solar cell output voltage (Volt), I_{SC} is short circuit current (Ampere), λ is irradiance (KW/m^2), λ_{ref} is reference irradiance (KW/m^2), T_C is solar cell temperature (Kelvin), K_I is Temperature coefficient, T_{ref} is the solar cell reference temperature (Kelvin), I_{RS} is reverse saturation current (Ampere), K is boltzmann constant (1.38x10^{-23}), A is the ideality factor, q is electron charge (1.6x10^{-19}Coulomb), and VOC is open circuit voltage (Volt).

Through the solar cell characteristic equation above, the relationship curve between output current (I_{PV}) and output voltage (V_{PV}) and the relationship curve between output power (P_{VP}) and output voltage V_{PV} can be obtained in a graph as in Fig. 3 [27].

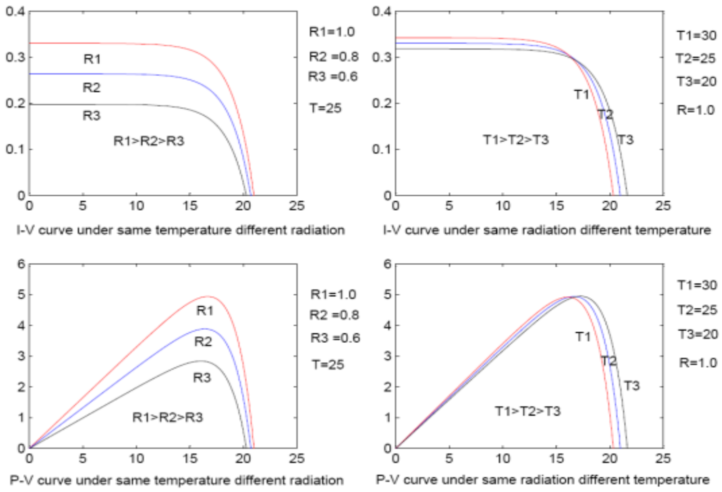

Fig. 3. I-V and P-V characteristic curves of solar

2.5 Stages of research

The research on "Maximum Power Point Tracker (MPPT) Based on the Inco Method in Solar Power Plants Using Buck-Boost DC-DC Converter" was conducted with the following stages [28][29].

1. Data collection, starting from literature review to observation, until obtaining a model that can be simulated, and incorporating the InCo algorithm into the MPPT simulation to determine the comparison of the initial and final values of the conducted simulation.
2. The design of the simulation represents the actual PV system using the datasheet. The simulation conducted in this research was carried out using the Simulink function from the MATLAB® R2016a software
3. Then, observe the variables such as the varying intensity of solar radiation and the surrounding temperature data by collecting data using a Digital Lux Meter. Then, the variable data is simulated into MATLAB® and Simulink® software to determine the maximum power achieved by the PV and the output power of the PV using the InCo algorithm.
4. Testing and analyzing the simulation results by conducting trials and evaluations of the created simulation. The test results will then be recorded and used as a reference for analysis.

2.6 Simulation design

System design is the initial step to determine the form of the system that will be created. The design stages are carried out so that when creating the system and simulating the system in the research, it can be realized in a structured, systematic, effective, and efficient manner. In the system design, it is divided into 3 main parts, namely:

1. Setting the PV parameters according to the original datasheet used in the PV system in the Pematang Johar area.The PV parameter uses only one panel of the monocrystalline type.
2. Design of buck-boost converter topology simulation in MATLAB® R2016a software.
3. Design of MPPT simulation using the InCo method in MATLAB® software.

2.7 Setting PV simulation

To conduct PV simulation testing on changes in solar radiation, a solar radiation model was created by measuring and monitoring the surrounding temperature in real-time. This figure was chosen because it shows the value of solar radiation during the hours of 09:00 AM to 04:00 PM Wib. Voltage and current will increase in the morning, reach their maximum in the afternoon, and start to decrease in the evening.

The PV module used in this simulation is the solar module. The PV module uses Standard Test Conditions (STC), which are the industry standard for testing the performance of PV modules by determining the cell surface temperature at 25°C and radiation at

1000 W/m², as well as using the I-V and P-V display characteristics of one module at 25°C and specified irradiances. The module is adjusted to the original PV module according to the specifications from the datasheet shown in Table 1.

Table 1. Data sheet of PV solar module

Modul Type	SP-330-M72
Rate Max Power (Pmax)	330 W
Current at Pmax (Imp)	8.59 A
Voltage at Pmax (Vmp)	38.4 V
Short Circuit Current (ISC)	9.11 A
Open Circuit Voltage (VOC)	47.3 V
Dimension (mm)	1956*992*40
Number of Cells	72
Max. System Voltage	1000 V
Temperature Range	-450C – 800C

From the specifications in Table 2, the solar modeling conducted uses a modeling structure that employs solar cells available in MATLAB® and Simulink® R2016a, created by the National Renewable Energy Laboratory (NREL) System Advisor Model (Jan. 2014). In general, this modeling is obtained from equations that have been adjusted to the characteristics of the PV itself. The parameters that need to be filled in to match the desired specifications of the PV module are as shown in Fig. 4.

Table 2. PV STC data sheet

All value is measured under STC	
AM	1.5
E	1000 W/m2
Tc	250C

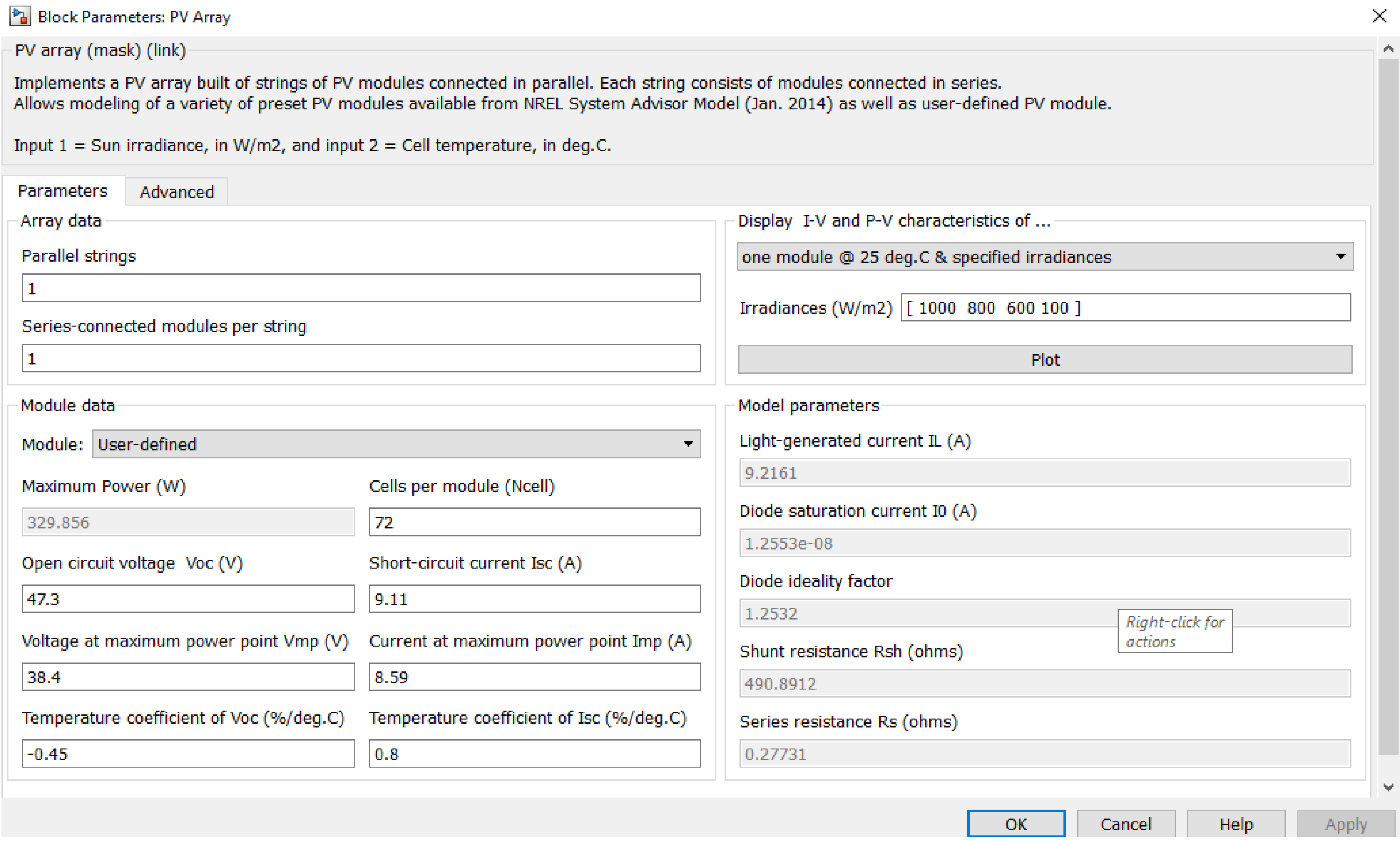

Fig. 4. Block parameter PV array

It seems there is no text to translate. Please provide the text you'd like me to translate, and I'll be happy to help! After entering the parameters according to the actual specifications of the PV module, the module can be tested with input parameters being temperature (T) and light intensity (Ir). The validation and estimation tests conducted involved providing the existing input parameters, namely temperature and light intensity, as well as the load. After it was done, the desired results were obtained.

After it was done, the desired results were obtained. The PV solar module has current and voltage characteristics that are in line with those of PV modules in general. A PV solar module has current and voltage characteristics that are consistent with PV systems in general. These characteristics can be seen through the I-V and P-V curves of the model. The I-V and P-V curves are formed to observe the changes in current and power of the PV cell when the voltage increases linearly and continuously until it reaches the Voc voltage point.

The values of radiation and temperature that will be inputs in the PV design according to STC. The simulation results show the graph of the relationship between current and voltage of the PV model, which can be seen in Fig. 5. The graph of the relationship between power and voltage from the PV model can be seen in Fig. 6.

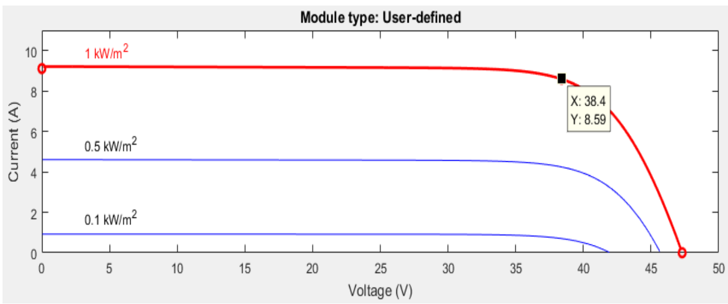

Fig. 5. Relationship between current and voltage

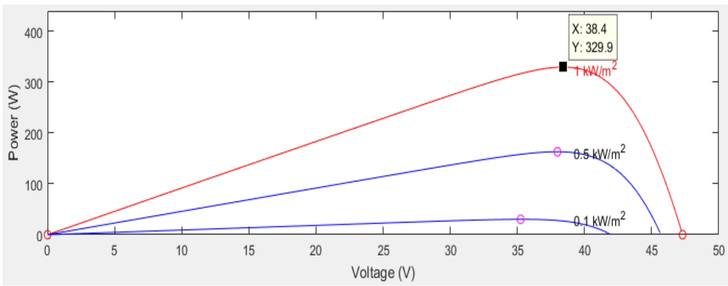

Fig. 6. Relationship between power and voltage

2.8 Designing a buck-boost converter simulation

The buck-boost converter (Fig. 7) used employs Pulse Width Modulation (PWM) control, where the buck-boost converter functions to regulate the input voltage to a more stable output voltage. There are several main components used in the buck-boost converter circuit, namely the MOSFET, diode, toroidal inductor, and capacitor. Where the MOSFET functions as a switch, and switching control is used using PWM. PWM switching can operate using the MPPT InCo algorithm. The change in output voltage is due to the difference in duty cycle.

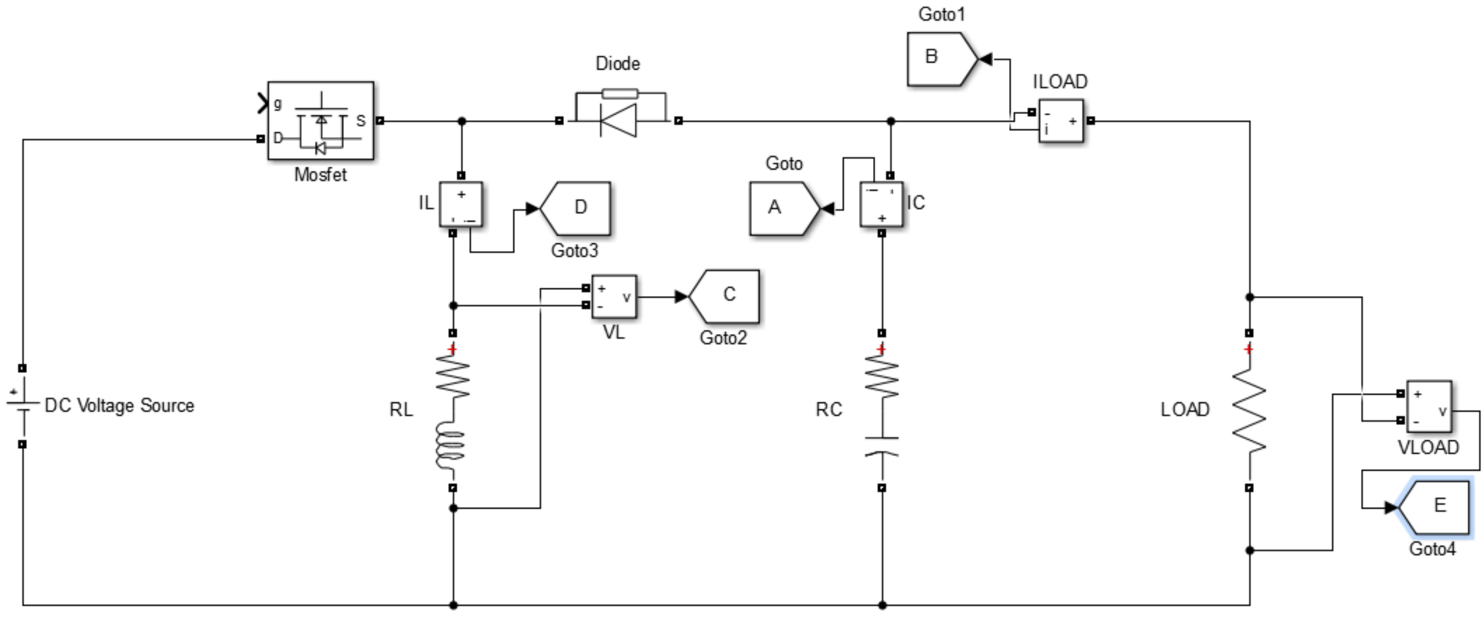

Fig. 7. Buck-boost converter topology

3 Results and discussion

3.1 Role of MPPT implementation of InCo method

In the previous chapter, the basic principle of the InCo method has been explained. It is said that this algorithm is a type of direct MPPT because it provides a reference to the maximum working point based on the voltage and current coming from the PV. InCo algorithm simulation chart can be seen in Fig. 8.

This algorithm is relatively simple but has good capability to find the maximum working point. In the InCo algorithm, there are two conditions where between (d~=) and (di>0, di<0). When (d~=0), then the algorithm will run to the increase duty area (d=d+0.001) with calculation Ipv + V_{PV} x (di/dv) <0, then decrease duty (d=d-0.001) Ipv + V_{PV} x (di/dv)>0, and the algorithm can directly calculate to the return area (repetition) of the final value (Vpre = V_{PV}) and (Ipre = Ipv). The next condition (di>0, di<0) the algorithm will run if di>0 then increase duty (d=d+0.001) then if di<0 then the algorithm becomes decrease duty (d=d-0.001) or the algorithm runs directly to the return area (repetition) of the final value (Vpre = V_{PV}) and (Ipre = Ipv). When performing a simulation, it is crucial to carefully set the required parameters to minimize the risk of simulation failure.

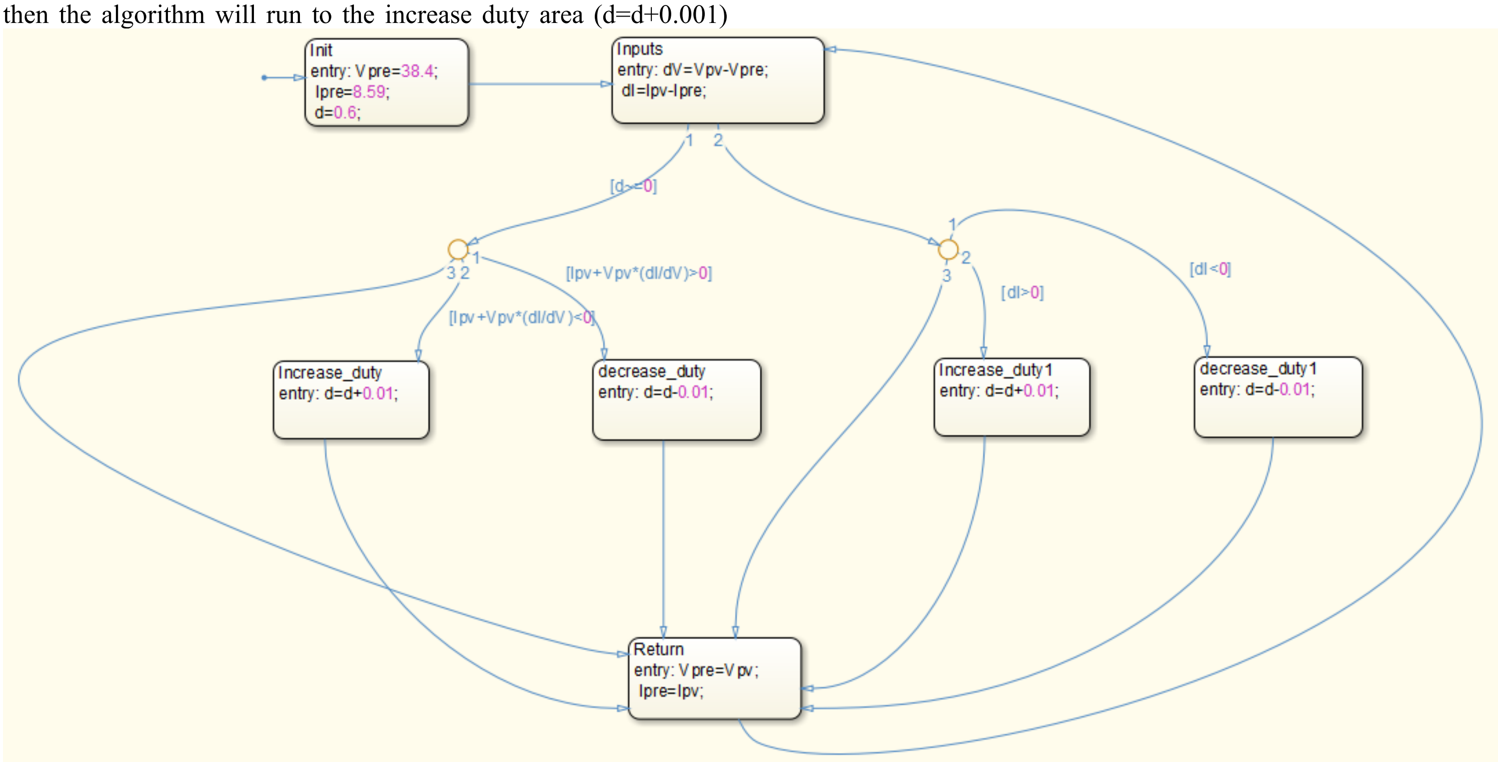

Fig. 8. InCo algorithm simulation

The simulation is conducted using MATLAB® and Simulink® software, utilizing datasheets from actual PV systems. Temperature and solar radiation data were collected using temperature measurements with a mini digital temperature and humidity sensor in the Pematang Johar area. Data collection is carried out during periods of optimal PV performance to ensure the accuracy and reliability of the simulation results. Simulation using MPPT and without MPPT can be seen in Figs. 9 and 10. Comparison graphs of the highest and lowest temperatures and irradiation can be seen in Figs. 11 and 12.

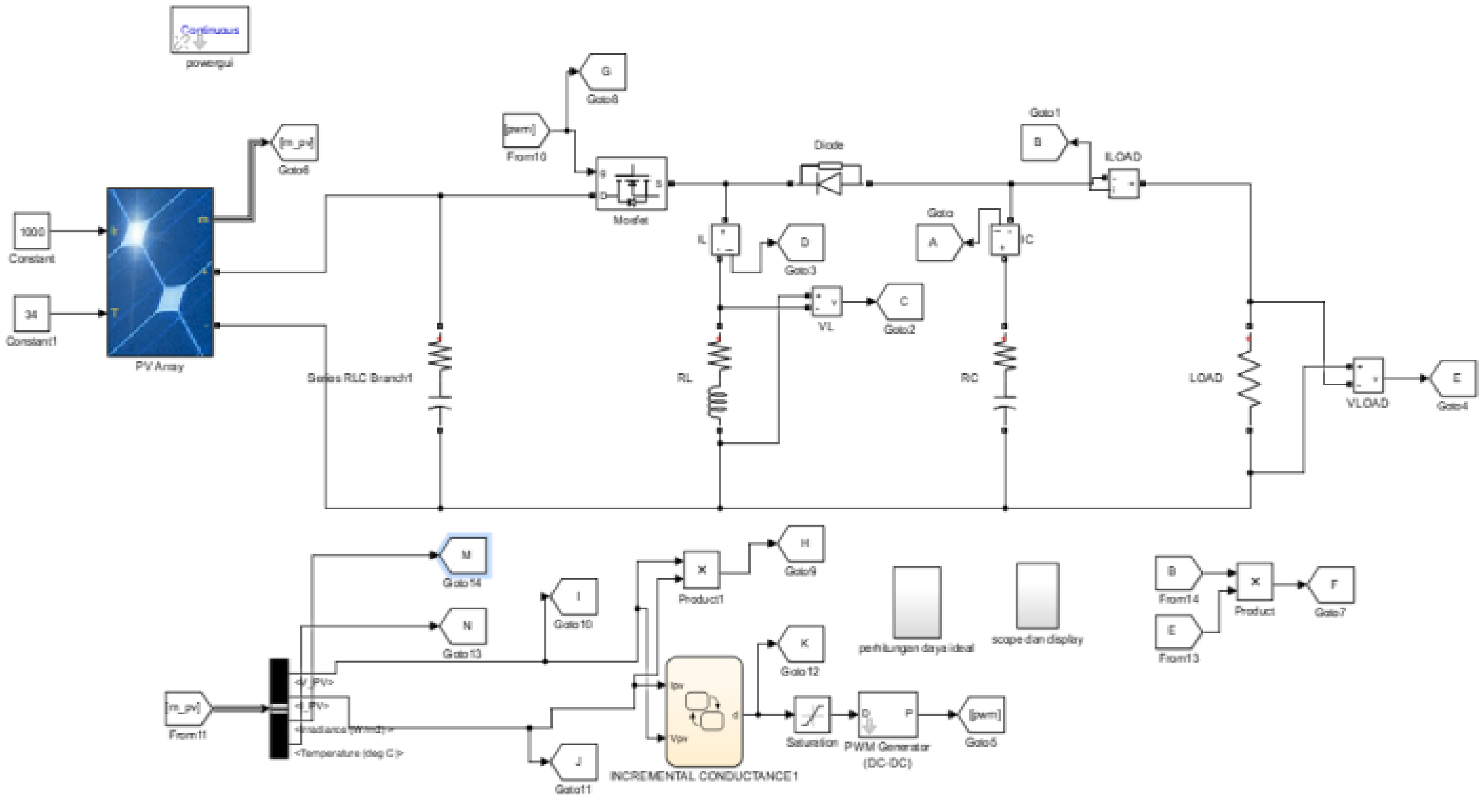

Fig. 9. Simulation using MPPT

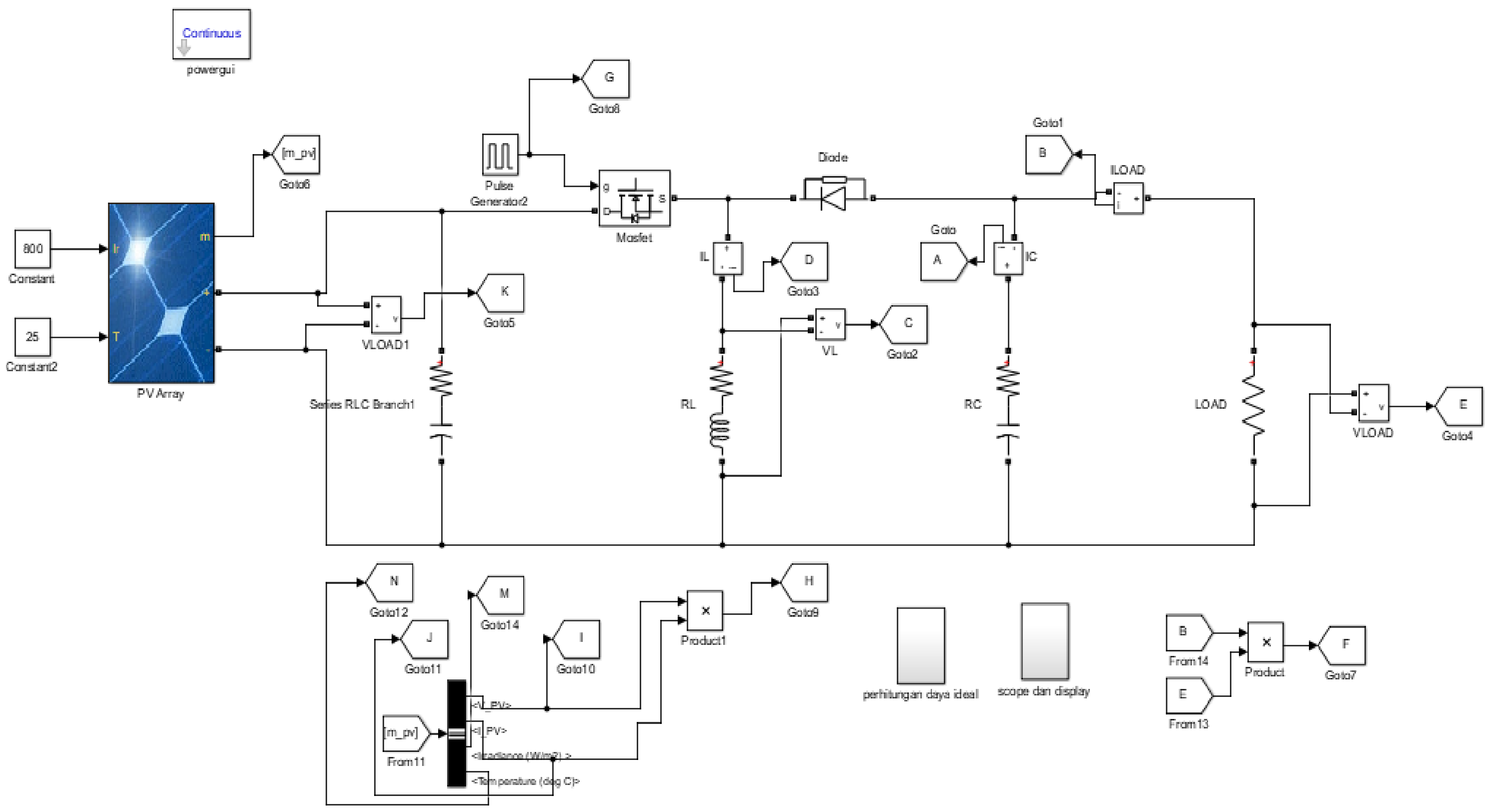

Fig. 10. Simulation without using MPPT

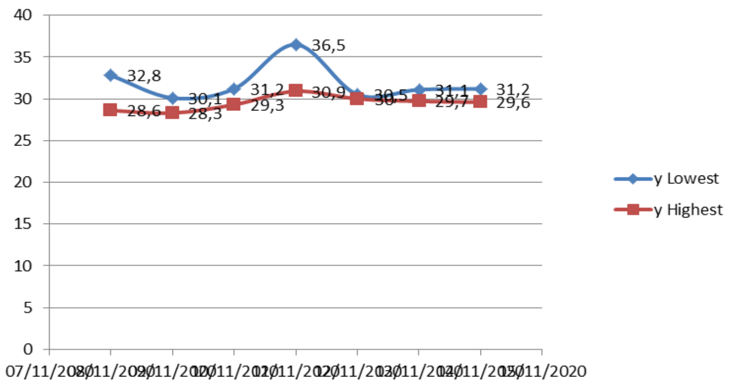

Fig. 11. Comparison graph of the highest and lowest temperatures

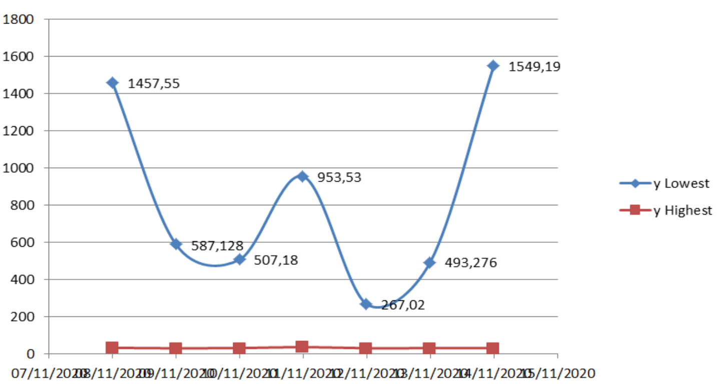

Fig. 12. Comparison graph of the highest and lowest irradiation

In Fig. 12, the highest irradiation value is shown in the red line, with the maximum value occurring in Fig. 12. The comparison graph of the highest and lowest irradiation occurred on November 14, 2020, amounting to 1549.19 W/m^2 [30]. While the lowest value occurred on November 12, 2020, amounting to 82,792 W/m2.

3.2 Analysis of InCo algorithm method (MPPT)

3.2.1 Incremental algorithm analysis method A

The testing of this system uses a PV system simulation that is adjusted to the datasheet, then directly connected to the buck-boost converter and MPPT system. In the InCo algorithm testing, it is done by entering logic in the form of a diagram that can be simulated. This testing is done by distinguishing into several methods, namely method A, namely (di>0, di<0), method B without MPPT, and method D, namely (d~=) with a frequency signal of 15,000 Hz.

3.2.2 Graph analysis of simulation results (Method A)

Fig. 13 presents the simulation results showing the Ipv graph in blue using the Bilevel Measurement method under a transition condition. The waveform exhibits a high value of 1.724e+00 and a low value of 1.724e+00, resulting in a small amplitude of 2.743e-05. On the positive edge, there are 22 rising edges with a rise time of 10.409 µs and a slew rate of 2.109 (/s). On the negative edge, there are 21 falling edges with a fall time of 14.210 µs and a slew rate of -1.544 (/s). The overshoot and undershoot characteristics are as follows: on the upper side, preshoot is 0.667%, overshoot is 32.667%, and undershoot is -0.597%; on the lower side, preshoot is 32.667%, overshoot is -0.667%, and undershoot is 0.667%. The waveform cycle has a period of 66.700 µs and a frequency of 14.993 kHz. On the upper side, there are 21 pulses with a pulse width of 36.690 µs and a duty cycle of 59.506%. On the lower side, there are also 21 pulses, with a width of 27.010 µs and a duty cycle of 40.494%.

The I_{out} waveform is shown in red, also using the Bilevel Measurement method under transition conditions. It shows a high value of 1.167e+00 and a low value of 5.806e-01, resulting in an amplitude of 5.864e-01. The positive edge contains 21 rising edges, a rise time of 17.796 µs, and a slew rate of 26.404 (/ms). The negative edge also has 21 falling edges with a fall time of 34.940 µs and a slew rate of -13.427 (/ms). The waveform shows symmetric overshoot values: both the positive and negative sides exhibit preshoot, overshoot, and undershoot of ±0.505%. The waveform cycle has a period of 66.700 µs and a frequency of 14.993 kHz. On the upper side, there are 21 pulses with a width of 29.637 µs and a duty cycle of 44.433%, while the lower side has 20 pulses with a width of 37.063 µs and a duty cycle of 55.567%.

Fig. 13. displays the Ppv waveform in blue, measured using the Bilevel Measurement method. Under transition conditions, it reaches a high value of 4.764e+00 and a low value of 4.346e+00, giving an amplitude of 4.180e-01. The positive edge includes 21 rising edges, a rise time of 23.642 µs, and a slew rate of 14.144 (/ms). On the negative edge, there are 21 falling edges with a fall time of 10.448 µs and a slew rate of -32.006 (/ms). The overshoot values on the upper side are: preshoot 0.649%, overshoot 29.221%, and undershoot -29.221%. On the lower side, preshoot is 29.221%, overshoot is -0.649%, and undershoot is 0.649%. The waveform has a period of 66.700 µs and a frequency of 14.993 kHz. The upper cycle includes 20 pulses with a width of 34.542 µs and a duty cycle of 51.760%, while the lower side has 21 pulses, a width of 32.176 µs, and a duty cycle of 48.240%.

The Pout waveform, shown in red, also applies the Bilevel Measurement under transition conditions, with a high value of 5.955e+00 and a low value of 1.491e+00, producing an amplitude of 4.464e+00. On the upper edge, the signal shows 21 rising edges, a rise time of 17.530 µs, and a slew rate of 203.729 (/ms). On the lower edge, it has 21 falling edges with a fall time of 33.195 µs and a slew rate of -107.587 (/ms). The overshoot analysis shows: upper side preshoot of 0.510%, overshoot of 1.531%, and undershoot of -1.531%; lower side preshoot of 1.531%, overshoot of -0.510%, and undershoot of 0.510%. The waveform's period is 66.700 µs with a frequency of 14.993 kHz**.** On the upper side, there are 20 pulses with a width of 26.356 µs and a duty cycle of 39.514%, while the lower side has 21 pulses, a width of 40.344 µs, and a duty cycle of 60.486%.

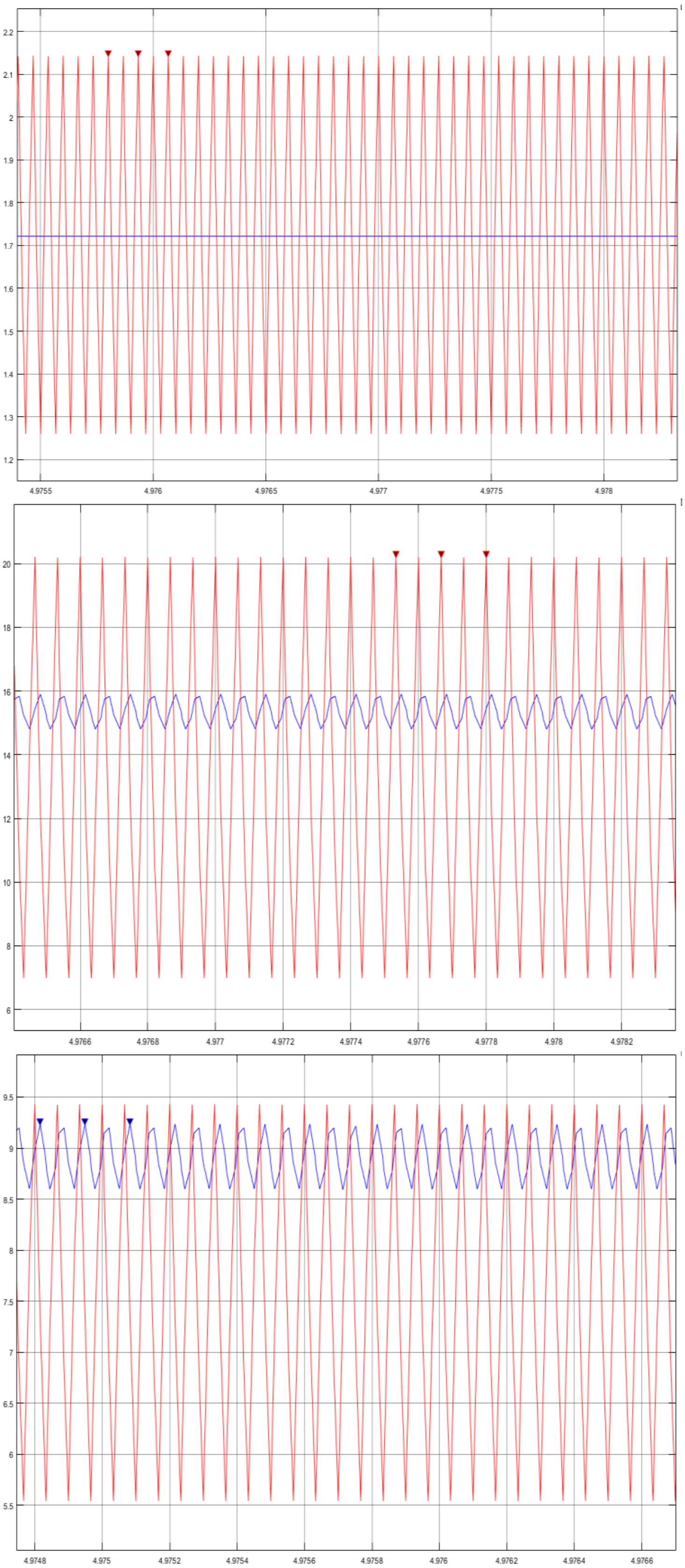

Fig. 13. P, V graph 13.00 day 1 method A

The V_{PV} waveform, shown in blue, is also measured using the Bilevel Measurement method. Under transition conditions, the high value is 2.764e+00 and the low value is 2.521e+00, resulting in an amplitude of 2.452e-01. The positive edge contains 21 rising edges, a rise time of 23.640 µs, and a slew rate of 8.206 (/ms). The negative edge shows 22 falling edges with a fall time of 10.447 µs and a slew rate of -18.569 (/ms). Overshoot and undershoot values on the upper side are: preshoot 0.649%, overshoot 29.221%, undershoot -29.221%. On the lower side, preshoot is 29.221%, overshoot is -0.649%, and undershoot is 0.649%. The waveform has a period of 66.700 µs and a frequency of 14.993 kHz. On the upper edge, there are 21 pulses with a width of 34.523 µs and a duty cycle of 51.759%, while on the lower edge, there are also 21 pulses with a width of 32.177 µs and a duty cycle of 48.241%.

The Vload waveform, measured using the Bilevel method, shows a transition with a high value of 5.135e+00 and a low value of 2.550e+00, resulting in an amplitude of 2.580e+00. On the positive edge, there are 21 rising edges, a rise time of 17.769 µs, and a slew rate of 116.176 (/ms). On the negative edge, there are 21 falling edges, a fall time of 34.940 µs, and a slew rate of -59.081 (/ms). Overshoot and undershoot values are identical on both sides: preshoot, overshoot, and undershoot are ±0.505%. The waveform cycle has a period of 66.700 µs and a frequency of 14.993 kHz. The upper edge contains 21 pulses with a width of 29.637 µs and a duty cycle of 44.433%, while the lower edge has 20 pulses, a width of 37.063 µs, and a duty cycle of 55.567%.

3.2.3 Incremental algorithm analysis method D

Using the D method (d~=), an InCo simulation was carried out over 5 seconds. The relationship between current, voltage, and power remains consistent across different irradiation and temperature settings, although the output values vary. However, this method experiences notable disturbances, with 27 recorded fluctuations during the 5-second run. These disturbances are mainly caused by low irradiation and non-optimal temperatures. Initially, the graph shows a smooth increase up to 1.42 seconds, corresponding to the PV output. Afterward, disturbances become frequent until the simulation ends. The D method helps maintain V_{PV} relative to irradiation and temperature variations, although it struggles under low solar input conditions, causing distortions in the output.

At a glance, Fig. 14 illustrates that the waveform exhibits similar ripple and rhythm patterns in the presence of disturbances. Upon initiating the simulation run, the graph shows an initial rise, which corresponds to the output value from the PV system. This iteration continues until 1.42 seconds during the run condition, after which the graph begins to show disturbances until the configured simulation period ends at 5 seconds.

Fig. 14 shows the I_{pv} waveform represented in blue. During the 1.42-second iteration, the Bilevel Measurement on the transition condition indicates a high value of 1.317e+00, a low of 1.298e+00, and an amplitude of 1.2938e-02. On the positive edge, the waveform exhibits +edges 416, +rise time of 19.566 µs, and a +slew rate of 792.474 (/s), while on the negative edge, –edges 416, -fall time of 13.791 µs, and a -slew rate of -1.124 (/ms) are observed. The Ipv waveform also shows overshoots/undershoots at 1.42 seconds, where on the upper side, +preshoot is 0.625%, +overshoot 24.375%, and +undershoot -0.242%, while on the lower side, –preshoot is 24.317%, -overshoot -0.625%, and -undershoot 0.625%. The signal cycle has a period of 66.667 µs and a frequency of 15.000 kHz, with +pulses 415, +width 39.388 µs, and +duty cycle 59.082%, while the negative side shows –pulses 416, -width 27.279 µs, and -duty cycle 40.918%.

Next, the Iout waveform shown in red under Bilevel Measurement indicates a transition with a high value of 3.604e+00, a low of 2.654e+00, and an amplitude of 9.501e-01. On the positive edge, it has +edges 416, +rise time 35.890 µs, and +slew rate of 21.177 (/ms), while the negative edge shows –edges 416, -fall time 15.161 µs, and -slew rate of -50.131 (/ms). The overshoot/undershoot values are symmetrical, with +preshoot, +overshoot, +undershoot all at 0.505%, and similar mirrored values on the negative side. The waveform cycle has a period of 66.667 µs and frequency of 15.000 kHz, with +pulses 415, +width 38.704 µs, +duty cycle 58.057%, and –pulses 416, -width 27.962 µs, -duty cycle 41.943%.

The Pvp graph in Fig. 14 shows a Bilevel Measurement with a transition at high 5.015e+01, low 4.924e+01, and amplitude 9.027e-01. On the positive edge, it shows +edges 416, +rise time 20.174 µs, and +slew rate 35.796 (/ms), while on the negative edge –edges 416, -fall time 13.862 µs, and -slew rate -52.094 (/ms). Overshoot/undershoot values on the upper side include +preshoot 30.906%, +overshoot 0.658%, and +undershoot -0.658%. On the lower side, –preshoot is 0.658%, -overshoot -0.004%, and -undershoot 30.921%. The signal cycle period is 66.667 µs with frequency 15.000 kHz, where +pulses are 416, +width 27.110 µs, +duty cycle 40.665%, and –pulses are 415, -width 39.556 µs, -duty cycle 59.335%.

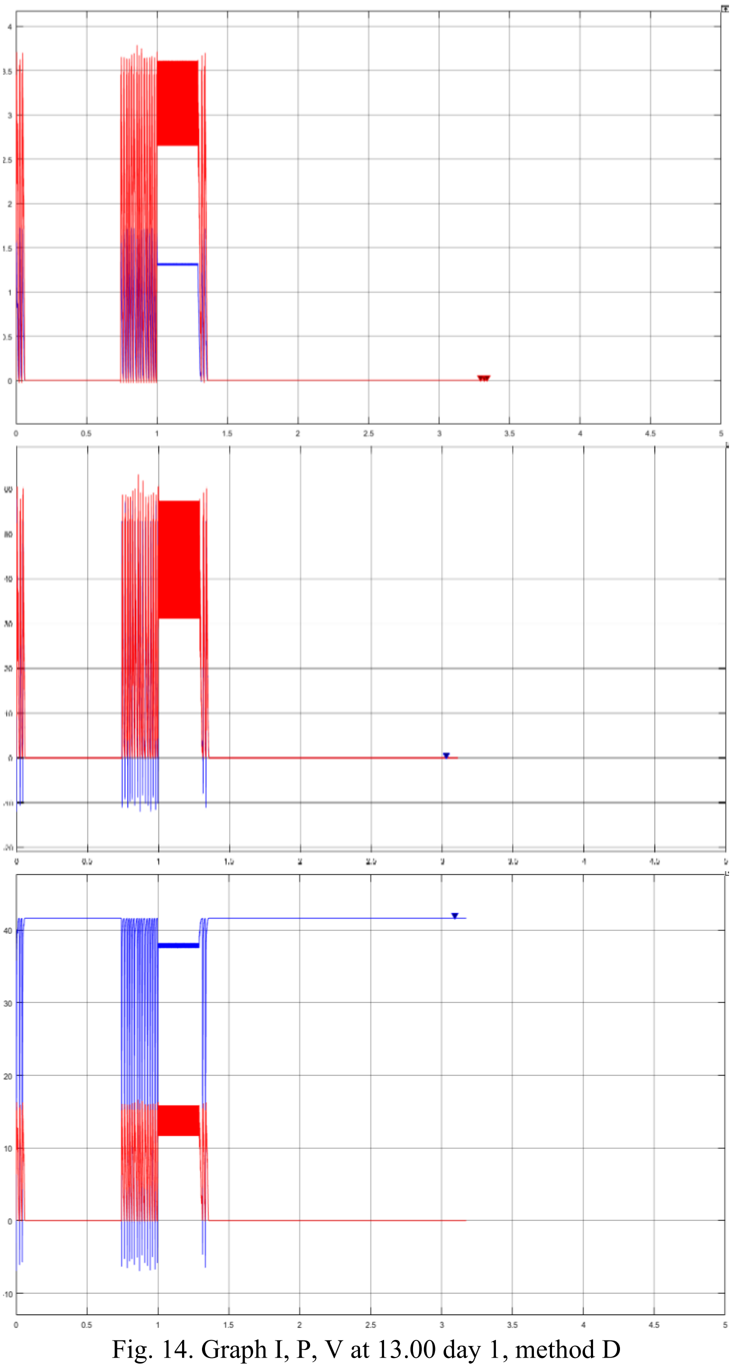

Fig. 14. Graph I, P, V at 13.00 day 1, method D

For the Pout waveform, the Bilevel Measurement indicates a transition with high 5.717e+01, low 3.101e+01, and amplitude 2.616e+01. The waveform shows +edges 416, +rise time 36.418 µs, +slew rate 574.630 (/ms), and –edges 416, -fall time 14.949 µs, -slew rate -1.400 (/µs). Overshoots and undershoots are symmetrical with values of ±0.505%. The signal cycle is recorded at a period of 66.667 µs, frequency 15.000 kHz, with +pulses 415, +width 36.355 µs, +duty cycle 54.533%, and –pulses 416, -width 30.312 µs, -duty cycle 45.467%.

In the V_{PV} graph (blue) shown in Fig. 14, the Bilevel Measurement records a transition with high 3.795e+01, low 3.754e+01, and amplitude 4.101e-01. On the positive side, it exhibits +edges 416, +rise time 13.764 µs, and +slew rate 23.838 (/ms), while the negative side shows –edges 416, -fall time 10.460 µs, and -slew rate -31.366 (/ms). Overshoot/undershoot values are: +preshoot 0.833%, +overshoot 65.833%, and +undershoot 0.692% on the upper side, while –preshoot is 65.833%, -overshoot -0.272%, and -undershoot 0.272% on the lower side. The cycle has a period of 66.667 µs, frequency of 15.000 kHz, with +pulses 415, +width 35.864 µs, +duty cycle 53.769%, and –pulses 416, -width 30.802 µs, -duty cycle 46.204%.

Lastly, the V_{out} graph (red) in Fig. 14 shows a Bilevel Measurement transition with high 1.586e+01, low 1.168e+01, and amplitude 4.180e+00. On the upper side, it has +edges 415, +rise time 35.890 µs, and +slew rate 93.180 (/ms), while on the lower side, –edges 416, -fall time 15.161 µs, and -slew rate -220.578 (/ms). Overshoot/undershoot values are consistent on both edges at ±0.505%. The waveform cycle has a period of 66.667 µs and a frequency of 15.000 kHz, with +pulses 415, +width 38.704 µs, +duty cycle 58.057%, and –pulses 415, -width 27.962 µs, -duty cycle 41.943%.

From the simulation results shown, a similarity is observed between Method A and Method D under the same irradiance and temperature conditions— (1457.55 W/m², 32.8 °C), (1549.19 W/m², 31.2 °C), and (1391.19 W/m², 30.9 °C)—despite the difference in the InCo duty applied in each simulated method.

3.3 Results of the InCo algorithm

The results of the InCo algorithm that have been analyzed in two methods will take the optimal results marked in red and green, and then the calculation will be carried out using the average value equation of V_{out} (Fig. 15), I_{out} (Fig. 16), P_{out} (Fig. 17), MPPT, and without MPPT.

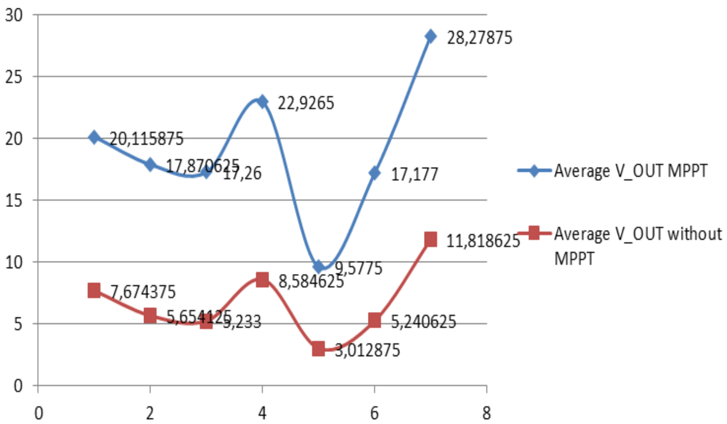

Fig. 15. Average V_{out} graph of optimal MPPT and without MPPT

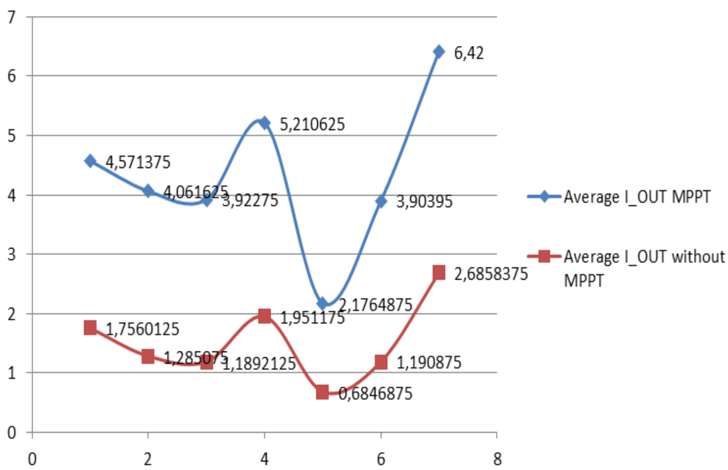

Fig. 16. Average I_{out} graph of optimal MPPT and without MPPT

The simulation results show that under varying irradiation conditions, the MPPT successfully tracks the maximum power output. The InCo algorithm was analyzed to understand its operational characteristics and its effect on MPPT performance. The outcomes from two different analysis methods are highlighted in red and green to indicate the optimal results. Subsequently, the average values of V_{out}, I_{out}, and Pout for both with and without MPPT were calculated using the corresponding average value equations.

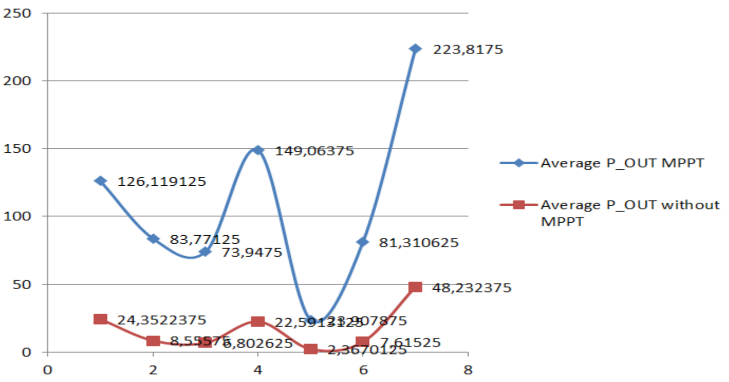

Fig. 17. Average P_{out} graph of optimal MPPT and without MPPT

4 Conclusion

This study demonstrates that integrating the InCo algorithm with a Buck-Boost DC-DC converter improves the performance of PV systems under variable irradiance and temperature conditions. The system was evaluated through simulation using several control methods. Method A, which applies the InCo algorithm for both increasing (di > 0) and decreasing (di < 0) current slopes, achieved the most stable output with slight reductions in PV voltage (V_{PV}) and current (I_{pv}). Method B, which excludes MPPT, consistently underperformed across all conditions, validating the necessity of dynamic tracking for optimal energy harvesting. Method D, which targets dV/dI ≈ 0 using a 15,000 Hz switching frequency, maintained higher V_{PV} but exhibited instability in output power under fluctuating irradiance. Simulation results revealed that the system with MPPT achieved average gains of 65.53% in voltage, 65.48% in current, and 86.47% in power compared to the non-MPPT configuration. However, a notable risk of output instability was observed when irradiance fell below ±300 W/m², highlighting the need for enhanced control strategies or protective circuits. The use of the InCo algorithm combined with a Buck-Boost converter offers a reliable and adaptive solution for PV power optimization.

References:

[1] A. Saleh, W. Hadi, and M. C. Anwar, "Desain Kontrol Maximum Power Point Traker (Mppt) Menggunakan Incremental Conductance (Inc) Pada Dc / Dc Tipe Sepic," *Semin. Nas. Sains dan Teknol. Fak. Tek. Univ. Muhammadiyah*, no. November, pp. 1–8, 2017.

[2] A. Safari and S. Mekhilef, "Incremental conductance MPPT method for PV systems," *Can. Conf. Electr. Comput. Eng.*, pp. 000345–000347, 2011, doi: 10.1109/CCECE.2011.6030470.

[3] S. S. Bulle, S. D. Patil, and V. V. Kheradkar, "Implementation of incremental conductance method for MPPT using SEPIC converter," *Proc. IEEE Int. Conf. Circuit, Power Comput. Technol. ICCPCT 2017*, 2017, doi: 10.1109/ICCPCT.2017.8074234.

[4] D. Menniti, A. Burgio, N. Sorrentino, A. Pinnarelli, and G. Brusco, "An incremental conductance method with variable step size for MPPT: Design and implementation," *2009 10th Int. Conf. Electr. Power Qual. Util. EPQU'09*, pp. 2–6, 2009, doi: 10.1109/EPQU.2009.5318833.

[5] . R., A. Azis Hutasuhut1, and Y. Chaniago, "Analysis of Hybrid Power Plant Technology Using Data Weather in North Sumatera," *Int. J. Eng. Technol.*, vol. 7, no. 4.7, p. 481, 2018, doi: 10.14419/ijet.v7i4.7.27364.

[6] P. Harahap, I. Nofri, and S. Lubis, "PLTS 200 Wp to Meet Energy Needs at the Taqwa Muhammadiyah Mosque, Sei Litur Village, Sawit Sebrang Langkat District," *J. Innov. Community Engagem.*, vol. 1, no. 1, pp. 60–71, 2021, doi: 10.28932/jice.v1i1.3380.

[7] P. Harahap, F. I. Pasaribu, C. A. P. Siregar, and B.

Oktrialdi, "Performance of Grid-Connected Rooftop Solar PV System for Households during Covid-19 Pandemic," *J. Electr. Technol. UMY*, vol. 5, no. 1, pp. 26–31, 2021, doi: 10.18196/jet.v5i1.12089.
[8] Rimbawati, M. A. Siregar, Z. Siagian, J. Riandra, P. Harahap, and B. Oktrialdi, "Lightning Arrester Design as a Security System for Photovoltaic Systems in Pematang Johar Village," *Proceeding - ELTICOM 2022 6th Int. Conf. Electr. Telecommun. Comput. Eng. 2022*, pp. 54–59, 2022, doi: 10.1109/ELTICOM57747.2022.10038261.
[9] B. Sabir, S. Der Lu, H. D. Liu, C. H. Lin, A. Sarwar, and L. Y. Huang, "A Novel Isolated Intelligent Adjustable Buck-Boost Converter with Hill Climbing MPPT Algorithm for Solar Power Systems," *Processes*, vol. 11, no. 4, 2023, doi: 10.3390/pr11041010.
[10] Z. Tang, Y. Zhang, and P. Davari, "Programmable Multi-input Buck-Boost Converter for Photovoltaics Arrays," *2024 IEEE 10th Int. Power Electron. Motion Control Conf. IPEMC 2024 ECCE Asia*, pp. 2589–2593, 2024, doi: 10.1109/IPEMC-ECCEAsia60879.2024.10567856.
[11] D. López del Moral, A. Barrado, M. Sanz, A. Lázaro, C. Fernández, and P. Zumel, "Analysis and implementation of the Autotransformer Forward-Flyback converter applied to photovoltaic systems," *Sol. Energy*, vol. 194, no. Mic, pp. 995–1012, 2019, doi: 10.1016/j.solener.2019.10.082.
[12] A. Muhammad, A. Amin, M. A. Qureshi, A. R. Bhatti, and M. M. Ali, "Deep learning based buck-boost converter for PV modules," *Heliyon*, vol. 10, no. 5, pp. 4–7, 2024, doi: 10.1016/j.heliyon.2024.e27405.
[13] N. Obeidi, M. Kermadi, B. Belmadani, A. Allag, L. Achour, and S. Mekhilef, "A Current Sensorless Control of Buck-Boost Converter for Maximum Power Point Tracking in Photovoltaic Applications," *Energies*, vol. 15, no. 20, 2022, doi: 10.3390/en15207811.
[14] F. I. Pasaribu, N. Evalina, and P. Harahap, "Varistor in the Inverator Circuit Starting Energy Saver to Reduce Water Pump Electric Current," pp. 244–253, 2017.
[15] G. S. Putra and M. Yuhendri, "Implementasi Sistem Kendali MPPT Panel Surya Berbasis Algoritma Incremental Conductance," *JTEIN J. Tek. Elektro Indones.*, vol. 1, no. 2, pp. 218–223, 2020.
[16] E. Sunarno, I. Sudiharto, and D. Yolanita, "Design MPPT with Anfis Method on Zeta Converter With DC Load," *Kinet. Game Technol. Inf. Syst. Comput. Network, Comput. Electron. Control*, vol. 4, no. 1, 2023, doi: 10.22219/kinetik.v8i1.1629.
[17] B. Shah Student, ad Vidya, S. Kureshi Student, M. Manubarwala Student, M. Maurya Student, and D. Gosai, "Fabrication and Testing of Solar Smart Bicycle," vol. 10, no. 5, pp. 259–264, 2019, [Online]. Available: http://www.ijser.org
[18] A. Badawi, H. Ali, I. M. Elzein, A. Zyoud, and A. Abu-Hudrouss, "Highly Efficient Pure Sine Wave Inverter Using Microcontroller for Photovoltaic Applications," *2023 Int. Symp. Networks, Comput. Commun. ISNCC 2023*, pp. 10–13, 2023, doi: 10.1109/ISNCC58260.2023.10323997.
[19] T. Mesin, E. Terbarukan, and T. Elektronika, "Ligh Rangkaian Panel Surya secara 300L Solar Water Heater 300L Solar Water Heater," pp. 1–8, 2021.
[20] E. Y. Setyawan, Y. I. Nakhoda, B. Widodo, and C. Soleh, "Alat Kontrol Temperatur Menggunakan Panel Surya untuk Mengurangi Tingkat Kematian pada Pembenihan Ikan Lele di Kabupaten Kediri," *J. Pengabdi. Pada Masy.*, vol. 4, no. 3, pp. 313–320, 2019, doi: 10.30653/002.201943.159.
[21] A. M. Mengenal, P. Sistem, P. Surya, O. Grid, and O. Grid, "Mengenal Perbedaan Sistem Panel Surya On Grid dan Off Grid," pp. 3–6, 2020.
[22] B. S. Mahdi, M. A. Al-fadheeli, N. bin Sulaiman, H. bin Hizam, S. bin Shafie, and M. A. Shehab, "Comparative Study of DC/AC Inverter Control Techniques for Three Phase Grid Connected PV System," *TEM J.*, vol. 11, no. 3, pp. 1364–1375, 2022, doi: 10.18421/TEM113-47.
[23] S. Panneerselvam, K. Kandasamy, and C. Perumal, "Modelling and simulation of sinusoidal pulse width modulation controller for solar photovoltaic inverter to minimize the switching losses and improving the system efficiency," *Arch. Electr. Eng.*, vol. 71, no. 3, pp. 615–626, 2022, doi: 10.24425/aee.2022.141674.
[24] U. S. Utara and U. S. Utara, "Desain dan Implementasi Kontrol Suhu Otomatis pada Inkubator Berbasis Mikrokontroler Atmega8535," 2017.
[25] Z. P. Wijaya, "Perancangan set up karakterisasi panel surya," *e-Journal Umr.*, pp. 1–19, 2019, [Online]. Available: http://jurnal.umrah.ac.id/wp-content/uploads/gravity_forms/1-ec61c9cb232a03a96d0947c6478e525e/2015/09/Zulnisyah-Putra-Wijaya.pdf
[26] F. A. Hidayat, "Performance Brushless Direct Current Motoraxial Flux 3 Phase Double Stator on the Difference of Enamel Wire Type in Stator Coil," *Dielektrika*, vol. 7, no. 2, p. 94, 2020, doi: 10.29303/dielektrika.v7i2.244.
[27] S. Suhaeb, Y. Abd Djawad, H. Jaya, Ridwansyah, Sabran, and A. Risal, "Mikrokontroler dan Interface," *Buku Ajar Jur. Pendidik. Tek. Elektron. UNM*, pp. 2–3, 2017, [Online]. Available: https://scholar.google.co.id/scholar?hl=id&as_sdt=0%2C5&q=jurnal+artikel+ilmiah&btnG=
[28] D. Lan, Y. Wu, T. B. Soeiro, P. Granello, Z. Qin, and P. Bauer, "12-pulse Rectifier with DC-Side Buck Converter for Electric Vehicle Fast Charging," *IECON Proc. (Industrial Electron. Conf.*, vol. 2022-Octob, pp. 1–6, 2022, doi: 10.1109/IECON49645.2022.9968872.
[29] N. I. Nahin, M. Nafis, S. Prokash Biswas, M. Kamal Hosain, P. Das, and S. Haq, "Investigating the input power quality of multi-pulse AC-DC power converter fed induction motor drives," *Heliyon*, vol. 8, no. 12, p. e11733, 2022, doi: 10.1016/j.heliyon.2022.e11733.
[30] G. H. and R. Hargreaves, G.L., Hargreaves, "Journals by Subject Publish with us Article citations," *Agric. Benefits Senegal River Basin. J. Irrig. Drain. Eng.*, pp. 1–5, 1985, doi: 10.4236/oalib.1113070.

[28] K .suwito, suhanto, "Sistem Baterai Charging pada Solar Energy System dengan Buck Boost Converter untuk Berbagai Tingkat Pencahayaan Di Bandar Udara," J. Teknol. Penerbangan, vol. 1, p. 1, 2017.
[29] B. Majhi, "Analysis of Single-Phase SPWM Inverter," vol. 3, no. May, pp. 1793–1798, 2012.
[30] D. Nugraha, "Rancang Bangun Inverter Satu Fasa Dengan Dengan Modulasi Lebar Pulsa PWM Menggunakan Antarmuka Komputer," *Jtev (Jurnal Tek. Elektro Dan Vokasional)*, vol. 06, no. 01, pp. 340–351, 2020